RSC Advances

PAPER

View Article Online
View Journal | View Issue

Cite this: *RSC Adv.*, 2025, **15**, 41260

Synthesis of azulenyl-substituted gold(I)-carbene complexes and investigation of their anticancer activity

Martin C. Dietl, [a] Christopher Hüßler, [a] Matthias Scherr, [a] Zoé M. Frederiksen, [a] Jürgen Graf, [a] Frank Rominger,[a] Matthias Rudolph,[a] Isabella Caligiuri,[b] Laura Tripodi,[c] Flavio Rizzolio, [bc] Thomas Scattolin *[d] and A. Stephen K. Hashmi *[ae]

Received 16th September 2025
Accepted 6th October 2025

DOI: 10.1039/d5ra07020a

rsc.li/rsc-advances

The direct and atom economic synthesis of azulenyl-substituted gold(I) carbene complexes, based on the modular template synthesis using gold(I) isonitrile complexes and amine nucleophiles, is presented. First, two azulenyl-substituted isonitriles as ligands were synthesized from a functionalizable azulene derivative, the latter stemming from a gold-catalyzed dimerization of internal alkynes. These azulene-bound gold(I) isonitrile complexes allow the smooth nucleophilic attack by both aliphatic and aromatic amines. The newly synthesized azulene-substituted gold(I) carbene complexes were evaluated for *in vitro* anticancer activity against multiple human cancer cell lines. Six lead compounds demonstrated potent and selective cytotoxicity, exceeding that of cisplatin by at least an order of magnitude in resistant and aggressive cancer models. Structure–activity relationship analysis revealed that specific ligand modifications, such as the position of the azulene moiety tethered to the carbene unit or nitrogen-bound ethyl or cyclic groups, are critical for enhancing the anticancer activity.

Introduction

Azulene, the non-benzenoid isomer of naphthalene, consists of a fused five- and seven-membered ring system and represents a distinctive 10π-electron aromatic hydrocarbon.[1] Its unique electronic structure, marked by a pronounced dipole moment and non-alternant π-system, makes azulene an exceptional chromophore among small hydrocarbons, exhibiting an intriguing blue colour.[2] Azulene derivatives have found applications in organic materials,[2,3] molecular sensors,[4–6] photoswitches,[7] and in medicinal chemistry.[8,9] In coordination chemistry, azulene-containing isonitriles have been studied with various transition metals, including Cr(0),[10–14] Ru(II),[15] Co(II),[16] Au(I),[17] W(0),[14] as well as on gold surfaces.[16,18–20] Nevertheless, examples of azulene-tethered metal carbene complexes remain extremely scarce. To date, only a single report has described the conversion of azulene-tethered gold(I) isonitriles into carbene complexes *via* reaction with aliphatic amines,[21] based on methodologies developed by Chugaev,[22–24] Bonati and Minghetti.[25–27] Gold complexes, especially those coordinated to carbene ligands, have emerged as promising candidates in the search for novel anticancer agents.[28–38] These compounds often display potent activity against a broad range of tumour types, including those resistant to conventional treatments. Gold complexes act through different mechanisms, such as inhibition of thioredoxin reductase, disruption of redox homeostasis, and interference with mitochondrial function.[39,40] Importantly, antiproliferative activity in gold complexes is highly sensitive to structural variations, rendering the rational design of new ligand frameworks a decisive factor for advancing the field.

In this context, the incorporation of azulene into gold(I) carbene complexes is of particular interest. The non-alternant aromatic system introduces an atypical electronic distribution and significant polarity, which can potentially enhance properties relevant to biological applications, such as lipophilicity, membrane permeability and cellular uptake. Thus, azulene represents a promising alternative to conventional aryl scaffolds in gold-based drug design.

Herein, we report the first systematic study of azulene-tethered gold(I) carbene complexes. Building on our ongoing research on gold(I) carbene complexes,[41–54] we establish a general synthetic strategy to access this novel compound class

[a]*Organisch-Chemisches Institut, Heidelberg University, Im Neuenheimer Feld 270, 69120 Heidelberg, Germany. E-mail: hashmi@hashmi.de; Web: http://www.hashmi.de; Fax: (+49)-6221-54-4205*

[b]*Pathology Unit, Department of Molecular Biology and Translational Research, Centro di Riferimento Oncologico di Aviano (CRO), IRCCS, Via Franco Gallini 2, 33081, Aviano, Italy*

[c]*Dipartimento di Scienze Molecolari e Nanosistemi, Università Ca' Foscari, Campus Scientifico Via Torino 155, 30174, Venezia-Mestre, Italy*

[d]*Dipartimento di Scienze Chimiche, Università Degli Studi di Padova, Via Marzolo 1, 35131 Padova, Italy. E-mail: thomas.scattolin@unipd.it*

[e]*Chemistry Department, Faculty of Science, King Abdulaziz University, Jeddah 21589, Saudi Arabia*

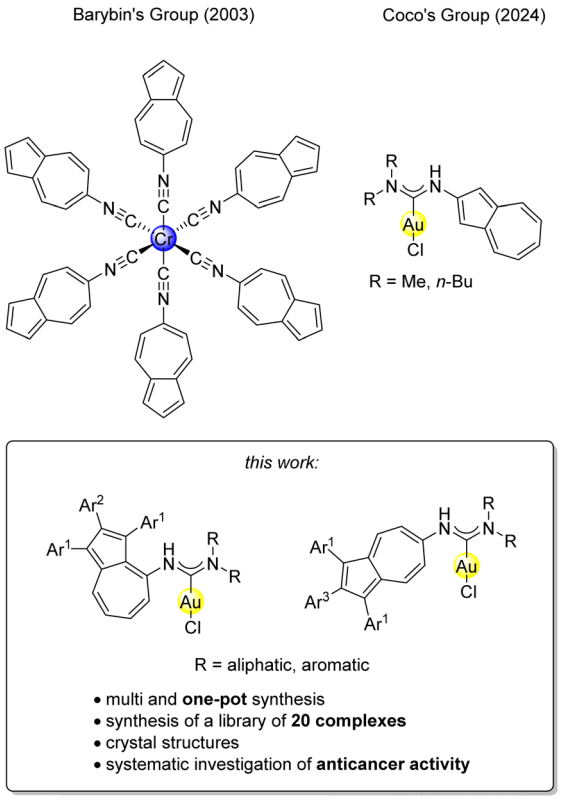

Fig. 1 Previous works by the group of Barybin[7] and Coco[12] concerning azulene-tethered metal complexes and description of this work.

and investigate their cytotoxic activity across a panel of human cancer cell lines (Fig. 1).

Results and discussion

The azulene-containing gold(I) complexes were synthesized *via* the isonitrile-based methodology from our group.[41–50] Starting from isonitrile gold(I) precursors, the use of different amines as nucleophiles allows for the systematic generation of a library of azulene-tethered gold(I) carbene complexes. This strategy offers a high degree of modularity, as structural variation can be achieved by variation of the nucleophile and the azulene-containing isonitrile. In contrast, alternative approaches, *e.g.*, *via* formamidinium salts require the preparation of a new precursor salt for each complex and therefore do not provide the same flexibility and efficiency.[55] The synthesis of the azulene core was developed in a previous study by our group.[56] Therein, a gold-catalyzed dimerization of push–pull diarylalkynes led to substituted azulenes. Therefore, we dimerized the internal alkynes **1a** and **1b** to form azulenes **2a** and **2b** used in this study in yields of 82% and 62%, respectively. As described,[56] substitution of a fluorine substituent attached to the azulene core by suitable nucleophiles is feasible. Previously, amination was achieved by reacting **2a** with ammonia (**3**) in glycol, affording the corresponding aminated azulene **4a**. However, since glycol can also act as a nucleophile under these conditions, the reaction not only led to the desired aminated product but also to the formation of a glycol ether–substituted azulene as a side product.[56] Our updated approach is presented here. Therein, **2a-b** were converted to the corresponding aminated azulenes **4a-b**, simply by reacting with 50 equivalents of a 25% aqueous solution of ammonia (**3**) in acetonitrile at 100 °C in a pressure vial. The reaction products **4a-b** were obtained selectively in a yield of 79% and 77% (Scheme 1). The successful displacement of the fluorine atom at the seven-membered rings of **2a-b** was proven both spectroscopically and by mass spectrometry. While **2a-b** depict resonances in the ^{19}F NMR spectra found at $\delta = -79.83$ and -82.89 ppm corresponding to the fluorine atom attached to the seven-membered ring of an azulene, this signal was not observed in **4a-b**, indicating a successful displacement by a nucleophile. In the ^{1}H NMR spectra of both substitution products, the resonances of the protons of the formed primary amine are visible at $\delta = 4.35$ ppm for **4a** and 3.21 ppm for **4b**.

After having obtained the aminated azulenes **4a-b**, a suitable reaction protocol for the conversion into the corresponding formamides was explored. The reaction of **4a** in toluene and formic acid at 110 °C, did not show any conversion of the starting material after 12 h. This lack of reactivity was attributed to the low nucleophilicity of the amino group of **4a**, since its free electron pair might show a stronger delocalization to the electron-deficient seven-membered ring of the azulene. In contrast, treatment of **4a** with acetic formic anhydride (**5**) in dichloromethane at room temperature, afforded complete conversion to the formamide **6a** within just 1 h. Under these conditions, the aminated azulenes **4a-b** were successfully converted into their corresponding *N*-formamides **6a-b** in a yield of 75% and 89% (Scheme 2). The introduction of the formamidyl-group was shown by the presence of the characteristic IR amide band at $\tilde{\nu}$= 1691 cm^{-1} for **6a** and $\tilde{\nu}$ = 1684 cm^{-1} for **6b**. Furthermore, the resonances of the formamidyl-group are both visible in the ^{1}H NMR and ^{13}C NMR spectra of **6a** and **6b**. In the ^{1}H NMR spectra, the resonance of the proton tethered to the nitrogen atom are found in the range between 7.40 and 8.08 ppm. Regarding the proton bound to the carbonyl moiety, its resonances are found in the ^{1}H NMR spectrum between 8.42 and 8.88 ppm, while the resonances of the carbonyl carbon atom are visible in the ^{13}C NMR spectra between 159.27 and 162.16 ppm. By slow diffusion of *n*-pentane into a concentrated solution of **6b** in 1,2-dichloroethane, single crystals suitable for an X-ray single crystal structure analysis were obtained. The molecular structure in the solid state shows the desired connectivity of all atoms, thereby verifying the successful formamidation of **4b** with acetic formic anhydride (**5**) to obtain the *N*-formamide **6b** (Fig. 2). To dehydrate the synthesized *N*-formamides **6a-b** to the corresponding isonitriles, suitable reaction conditions were subsequently investigated. Initial attempts to dehydrate **6b** using phosphoryl chloride and *iso*-propylamine in dichloromethane at room temperature did not result in any conversion.[40] Similarly, treatment of **6b** with the Burgess reagent, a mild dehydrating agent,[57] led to an unselective decomposition of the starting material after 12 h at room temperature. A microwave-assisted dehydration using cyanuric chloride and triethylamine in dichloromethane under microwave irradiation at 50 °C for 15 minutes showed only trace

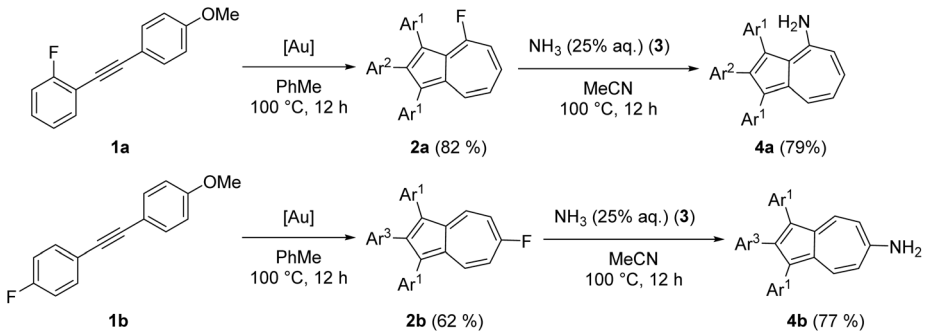

Scheme 1 Synthesis of amino-substituted azulenes **4a-b** from the azulenes **2a-b**, the latter deriving from the dimerization push–pull diarylalkynes **1a** or **1b**. Conditions: **1a-b** (1.00 eq.) [IPr*Au(NCMe)]SbF_6 (5 mol%), PhMe, 100 °C, 12 h; **2a-b** (1.00 eq.), **3** (50 eq., 25% aq.), MeCN, 100 °C, 12 h. Ar^1 = *para*-methoxyphenyl-, Ar^2 = *ortho*-fluorophenyl-, Ar^3 = *para*-fluorophenyl-.

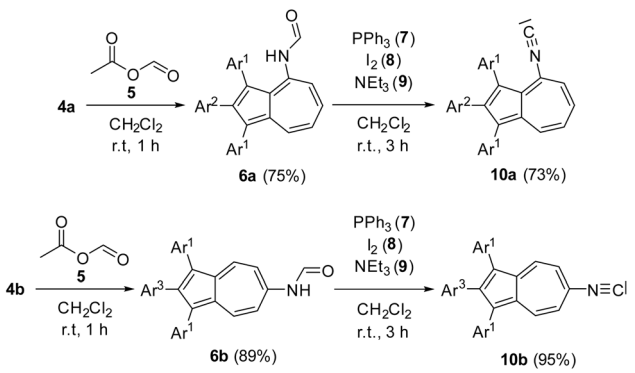

Scheme 2 Synthesis of azulene *N*-formamides **6a-b** from aminated azulenes **4a-b** and acetic formic anhydride (**5**) and the subsequent dehydration with triphenylphosphine (**7**), I_2 (**8**) and triethylamine (**9**) to azulene-tethered isonitriles **10a-b**. Conditions: **4a-b** (1.00 eq.), **5** (1.00 eq.), CH_2Cl_2, r.t., 1 h; **6a-b** (1.00 eq.), **7** (3.00 eq.), **8** (3.00 eq.), **9** (6.00 eq.), CH_2Cl_2, 1–3 h. Ar^1 = *para*-methoxyphenyl-, Ar^2 = *ortho*-fluorophenyl-, Ar^3 = *para*-fluorophenyl-.

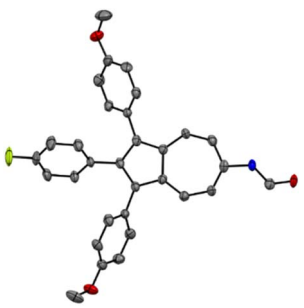

Fig. 2 ORTEP molecular solid-state structure of azulene *N*-formamide **6b** (CCDC 2449313). Thermal ellipsoids are shown with a 50% probability. Hydrogen atoms were omitted for clarity.

amounts of the desired isonitrile.[58] Only upon applying the method developed by the group of Danishefsky,[59] using triphosgene in dichloromethane at 0 °C, led to the formation of the desired isonitrile **10b** in 47% yield after 2 h. A further improvement was achieved using a protocol reported by the group of Luo for the synthesis of aromatic isonitriles.[60] With this method, **6b** was converted to the target isonitrile **10b** with triphenylphosphine (**7**), iodine (**8**), and triethylamine (**9**) in dichloromethane at room temperature in a yield of 95% after only 1 h. Given the higher yield, shorter reaction time, and use of less toxic reagents compared to triphosgene, all subsequent dehydrations of **6a-b** were carried out using this method yielding **10a** in 73% and **10b** in 95% (Scheme 2). The successful outcome of the dehydrations could be monitored by means of IR-spectroscopy. The IR-stretching mode of the formamidyl-groups of **6a-b** vanished, while the characteristic IR-stretching mode of the generated isonitrile group appeared at $\tilde{\nu}$ = 2109 cm^{-1} for **10a** and $\tilde{\nu}$ = 2108 cm^{-1} for **10b**.

Subsequently, isonitriles **10a** and **10b** were reacted with the commercially available [AuCl(DMS)] (**11**) in dichloromethane to afford the corresponding gold(I) complexes *via* ligand exchange. Full conversion of the starting material was observed after only 1 h by analysis of TLC. After purification by flash column chromatography, the corresponding gold(I) isonitrile complexes **12a** and **12b** were isolated in yields of 81% and 74%, respectively

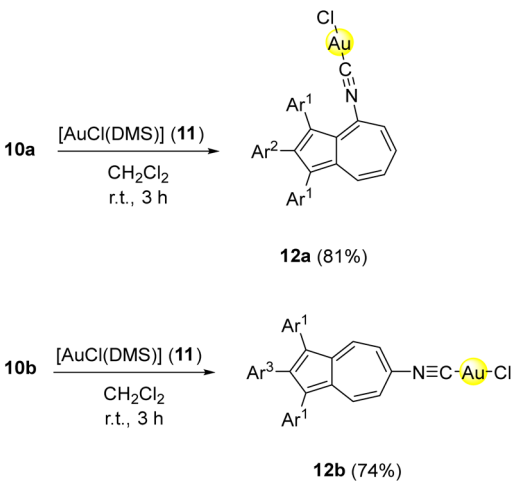

Scheme 3 Synthesis of azulene-tethered gold(I) isonitrile complexes **12a-b** from azulene-tethered isonitriles **10a-b** and [AuCl(DMS)] (**11**). Conditions: **10a-b** (1.00 eq.), **11** (1.00 eq.), CH_2Cl_2, r.t., 3 h. Ar^1 = *para*-methoxyphenyl-, Ar^2 = *ortho*-fluorophenyl-, Ar^3 = *para*-fluorophenyl-.

(Scheme 3). By slow diffusion of *n*-pentane into saturated solutions of **12a-b**, single crystals suitable for an X-ray single crystal structure analysis were obtained. Both molecular structures in the solid state show the successful coordination of the gold(I) metal centre to the isonitrile ligands **10a-b** in the linear coordination geometry typical for gold(I) (Fig. 3). However, no intermolecular aurophilic interactions[61–63] were observed in **12a** and **12b**.

The gold(I) isonitrile complexes **12a** and **12b** were then reacted with 1.05 eq. of various aliphatic and aromatic amines **13a-i** in dichloromethane at room temperature, affording the azulene-tethered gold(I) *N*-acyclic carbene complexes **14aa–ai** and **14ba–bi** in moderate to good yields (Scheme 4). The reactivity trends reflect differences in nucleophilicity and steric demand of the amines, as well as the steric properties of complexes **12a** and **12b**. Complex **12a**, where the azulenyl-ligand is tethered to the 4-position, is sterically more hindered than **12b**, resulting in lower yields of **14aa–ai** with 52–71% compared to **14ba–bi** with 68–91%. Nucleophilic and sterically less demanding amines, such as diethylamine (**13a**), pyrrolidine or piperidine (**13c**), gave the highest yields. In contrast, sterically encumbered aromatic amines like 2,6-dimethylaniline (**13d**), mesitylamine (**13e**) and 2,6-diisopropylaniline (**13f**) showed a decreased reactivity, leading to lower yields of 52–65% for **14ad–af** and 68–74% for **14bd–bf**. 2-Aminopyridine (**13g**) as a sterically not demanding but weakly nucleophilic amine, gave moderate yields of 63% for **14ag** and 77% for **14bg**. *N*-alkylated amines (**13h–i**) displayed enhanced nucleophilicity, improving the obtained yields relative to their primary analogues. The sterically demanding *iso*-propyl substituent in **13i** lowered yields with 65% for **14ai** and 80% for **14bi**, compared to the methyl-substituted analogue **13h** with yields of 71% for **14ah** and 88% for **14bh**.

The successful outcome of all reactions was assessed analytically by means of NMR, IR and UV-Vis spectroscopy and mass spectrometry. Bulk purity was determined to be over 95% of **14aa–ai** and **14ba–bi** by elemental analysis. While the starting materials **12a-b** both possessed an isonitrile group which depicted a characteristic band in the IR-spectra, after the addition of the amines in the IR-spectra of the gold(I) carbene complexes no signal belonging to the isonitrile moiety was observed. However, in the ^{13}C NMR spectra of **14aa–ai**, as well as **14ba–bi**, resonances between $\delta = 188.81$ ppm and 194.04 ppm were observed, that indicate the formation of a carbene centre. Furthermore, the resonances of the protons in the ^{1}H NMR spectra, as well as the high-resolution mass spectra indicate the successful formation of the desired gold(I) carbene complexes. Diffusion of *n*-pentane into saturated solutions of **14aa**, **14ba** and **14bd** led to single crystals suitable for X-ray diffraction (Fig. 4), that on top of the previously presented analytics confirm the proper connectivity of all atoms and hence prove the successful outcome of the reaction. The molecular structures in the solid state of **14aa**, **14ba** and **14bd** show the typical linear coordination geometry of gold(I) metal centres (Fig. 4). While no intermolecular aurophilic interactions[61–63] were observed for complexes **14aa** and **14ba**, compound **14bd** displayed a Au–Au distance of 3.2315(10) Å.

After the successful multistep synthesis of the azulenyl-substituted gold(I) carbene complexes **14aa–ai** and **14ba–bi**, the feasibility of a one-pot protocol was explored. This would offer a direct approach to the final products starting from the commercially available [AuCl(DMS)] (**11**), azulene containing isonitriles **10a-b** and aliphatic, as well as aromatic amines and consequently offer a greener approach to the formation of the desired reaction products, since workup steps of intermediates including organic solvents would be avoided. The feasibility of a one-pot approach was investigated with diethylamine **13a** and piperidine **13c** as examples of aliphatic amines, as well as 2,6-diisopropylaniline **13f** as an aromatic amine. Therefore, [AuCl(DMS)] **11** was firstly reacted with either **10a** or **10b** in dichloromethane for 1 h at room temperature. Afterwards, the respective amine was added to the reaction mixture. In all cases the full consumption of the starting materials was observed *via* analysis of TLC after an additional reaction time of 12 h. With the one-pot protocol, the azulenyl-substituted gold(I) carbene complexes **14aa**, **14ba**, **14ac**, **14bc**, **14af** and **14bf** were formed in similar yields compared to the multistep approach (Scheme 5). Overall, the one-pot approach offers a valuable, greener and more time economic alternative to a multistep synthesis towards the reaction products. After the successful multistep, as well as one-pot synthesis of azulene tethered gold(I) *N*-acyclic complexes **14aa**, **14ba**, **14ac**, **14bc**, **14af** and **14bf**, next an approach towards azulene-substituted gold(I) saturated *N*-heterocyclic carbene complexes[46–48] was evaluated. For this reason, the gold(I) isonitrile complexes **12a-b** were reacted with 1.05 equivalents of *N*-(2-chloroethyl)propan-2-amine hydrochloride (**15**), that was converted *in situ* to the reactive *N*-(2-chloroethyl)propan-2-amine by addition of triethylamine (**9**) as a base in dichloromethane for 12 h. The corresponding gold(I) saturated *N*-heterocyclic carbene complexes **16a-b** were obtained in moderate to good yields of 60% and 85%, respectively (Scheme 6). The discrepancy of the yields is again attributed to the steric demand of the azulenyl-tethered isonitrile at the starting material **12a-b**. UV-Vis absorption spectra of all and cyclic voltammetry of selected complexes were obtained and are available in the SI of this manuscript.

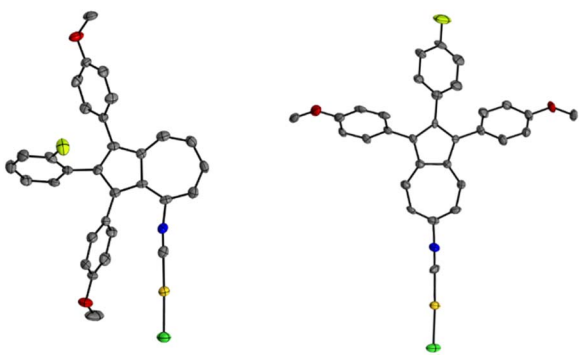

Fig. 3 ORTEP molecular solid-state structure of azulene-tethered gold(I) isonitrile complexes 12a (CCDC 2449314) and 12b (CCDC 2449315). Thermal ellipsoids are shown with a 50% probability. Hydrogen atoms were omitted for clarity.

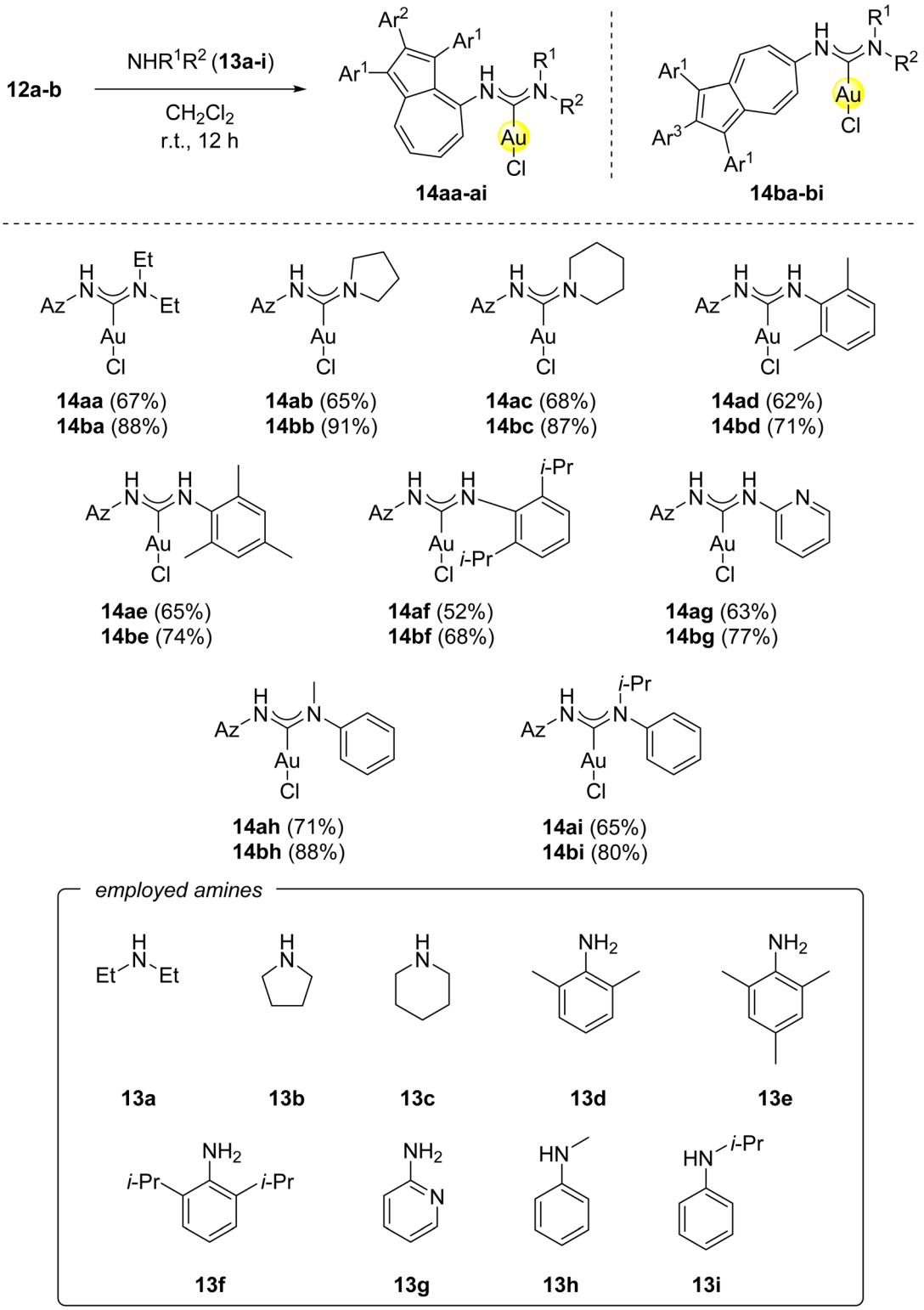

Scheme 4 Synthesis of azulene-tethered gold(I) *N*-acyclic carbene complexes **14aa–ai** and **14ba–bi** from azulene-tethered gold(I) isonitrile complexes **12a-b** and primary or secondary amines **13a–i**. Conditions: **12a-b** (1.00 eq.), **13a–i** (1.05–1.50 eq.), CH_2Cl_2, r.t., 12 h. Ar^1 = *para*-methoxyphenyl-, Ar^2 = *ortho*-fluorophenyl-, Ar^3 = *para*-fluorophenyl-.

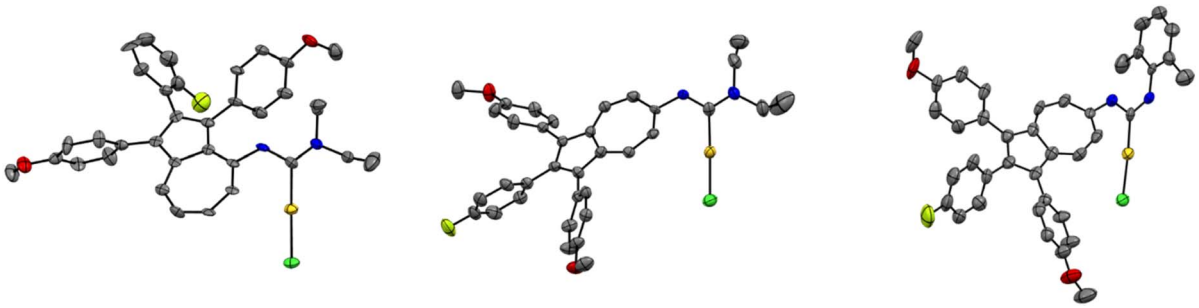

Fig. 4 ORTEP molecular solid-state structure of azulene-tethered gold(I) *N*-acyclic carbene complexes **14aa** (left) (CCDC 2449316), **14ba** (middle) (CCDC 2449317) and **14bd** (right) (CCDC 2449318). Thermal ellipsoids are shown with a 50% probability. Hydrogen atoms were omitted for clarity.

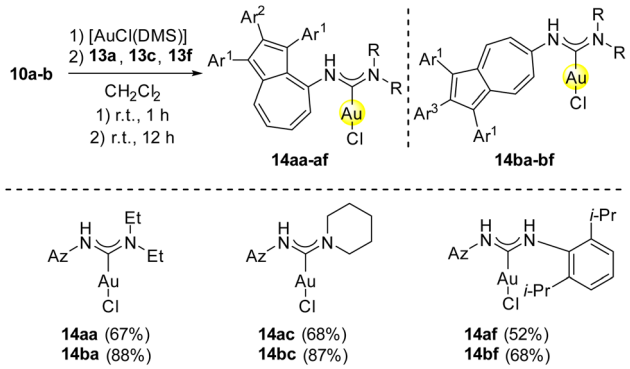

Scheme 5 One-pot synthesis of azulene-tethered gold(I) *N*-acyclic carbene complexes **14aa**, **14ba**, **14ac**, **14bc**, **14af** and **14bf** from [AuCl(DMS)] (**11**) azulene-tethered isonitriles **10a-b** and diethylamine (**13a**), piperidine (**13c**) and 2,6-diisopropylaniline (**13f**). Conditions: **11** (1.00 eq.), **10a-b** (1.00 eq.), **13a** (1.05 eq.), CH_2Cl_2, r.t., 13 h. Ar^1 = *para*-methoxyphenyl, Ar^2 = *ortho*-fluorophenyl, Ar^3 = *para*-fluorophenyl.

Anticancer activity of azulene-substituted gold(I)-carbene complexes

As anticipated in the introduction section, over the past two decades, interest in gold-based therapeutics has grown significantly, driven by their unique chemical properties and modes of action that differ markedly from traditional platinum-based drugs like cisplatin.[28–38] Unlike platinum complexes, which typically bind DNA directly, gold compounds tend to target proteins and enzymes, making them attractive for tackling cancers that have developed resistance to DNA-damaging agents. In particular, the high affinity of gold(I) for thiol and selenol groups renders it highly effective in targeting cysteine- and selenocysteine-containing proteins, which play central roles in redox regulation and cancer cell survival.[39,40]

Several gold compounds, such as auranofin, originally approved for the treatment of rheumatoid arthritis, have shown promising anticancer activity in both *in vitro* and *in vivo* models, prompting renewed interest in the medicinal chemistry of gold. Recent efforts have focused on the development of gold complexes with tailored ligands to modulate pharmacokinetic properties, cellular uptake, and target specificity.[28–38] Among these, *N*-heterocyclic carbene (NHC) ligands have emerged as particularly valuable due to their strong σ-donating ability, resistance to oxidation, and ease of structural modification.

Gold NHC complexes can be finely tuned to enhance lipophilicity, improve cellular permeability, or incorporate targeting moieties, thus enabling the development of more selective and less toxic anticancer agents.[28–38] Moreover, the modularity of carbene ligands allows for the rational design of compounds with dual or multi-target activity, which is increasingly recognized as a key strategy in addressing cancer heterogeneity and drug resistance.

With the aim of determining whether the wide range of azulenyl-substituted gold(I) carbene complexes synthesized in this work exhibit potential cytotoxicity, their *in vitro* anticancer activity was evaluated across a panel of human cancer cell lines. Prior to these investigations, the stability of representative

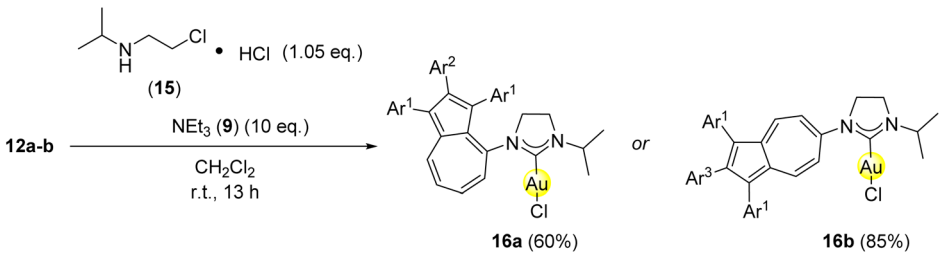

Scheme 6 Synthesis of azulene-tethered gold(I) saturated *N*-heterocyclic carbenes **16a-b** from azulene tethered isonitrile complexes **12a-b**, *N*-(2-chloroethyl)propan-2-amine hydrochloride (**15**) and triethylamine (**9**). Conditions: **12a-b** (1.00 eq.), **15** (1.05 eq.), **9** (10.0 eq.), CH_2Cl_2, r.t., 12 h. Ar^1 = *para*-methoxyphenyl-, Ar^2 = *ortho*-fluorophenyl-, Ar^3 = *para*-fluorophenyl-.

complexes was tested in the cell medium. Exemplarily, ^{1}H NMR spectra of **14ab** and **14ba** in a 100 mM saline solution in D_2O and DMSO-d_6 did not show signs of decomposition after 96 h at room temperature. This ensured that the subsequent tests reflected the properties of intact complexes. The investigated cell lines included A2780 (cisplatin-sensitive ovarian carcinoma), A2780*cis* (cisplatin-resistant ovarian carcinoma), MDA-MB-231 (triple-negative breast cancer), and U87 (glioblastoma).

For comparison, the cytotoxic profile of cisplatin, a widely used platinum-based chemotherapeutic, was determined under the same conditions.

These cell lines were selected to cover a range of cancer types with distinct biological and clinical relevance. A2780 and its cisplatin-resistant variant A2780*cis* provided a model to assess both chemosensitive and chemoresistant ovarian cancer phenotypes. The triple-negative breast cancer cell line MDA-MB-231 was included as a representative of an aggressive breast cancer subtype characterized by poor prognosis and limited therapeutic options. In addition, U87 cells were chosen as a well-established glioblastoma model, allowing us to explore the applicability of our approach in a central nervous system tumor setting. Taken together, this panel of cell lines was chosen to investigate the potential efficacy of our strategy across different tumor origins and resistance profiles.

The data obtained in this work, expressed as IC_{50} values and summarized in Table 1, clearly demonstrate that only a subset of the tested complexes exhibit significant cytotoxic activity, highlighting the substantial influence of carbene ligand decoration on antiproliferative effects. This observation suggests that subtle changes in ligand structure can markedly impact the biological performance of these gold(I) carbene complexes.

Table 1 Antiproliferative activity on A2780, A2780*cis*, MDA-MB-231 and U87 cancer cell lines[a]

	IC_{50} (μM)			
Compound	A2780	A2780*cis*	MDA-MB-231	U87
Cisplatin	2.5 ± 0.2	70 ± 10	60 ± 10	30 ± 10
14aa	3.4 ± 0.3	2.0 ± 0.6	0.95 ± 0.05	1.8 ± 0.2
14ba	7 ± 2	3 ± 1	1.4 ± 0.2	5.4 ± 0.2
14ab	3.5 ± 0.1	1.7 ± 0.2	1.7 ± 0.3	2.7 ± 0.3
14bb	80 ± 10	70 ± 10	70 ± 10	90 ± 10
14ac	4.1 ± 0.4	3 ± 1	3.2 ± 0.3	4.9 ± 0.1
14bc	70 ± 20	>100	25 ± 2	10 ± 2
14ad	90 ± 10	>100	>100	>100
14bd	>100	>100	>100	>100
14ae	>100	>100	>100	>100
14be	>100	>100	>100	>100
14af	>100	>100	>100	>100
14bf	>100	>100	>100	>100
14ag	80 ± 10	>100	80 ± 20	80 ± 10
14bg	>100	>100	40 ± 10	80 ± 20
14ah	70 ± 10	50 ± 20	9 ± 2	6.3 ± 0.2
14bh	70 ± 10	>100	10 ± 3	5.2 ± 0.3
14ai	80 ± 10	7.1 ± 0.1	3.8 ± 0.7	17 ± 4
14bi	80 ± 10	30 ± 1	15 ± 3	14 ± 1
16a	4.7 ± 0.2	1.1 ± 0.4	1.0 ± 0.2	1.5 ± 0.5
16b	8 ± 1	3.3 ± 0.7	3 ± 1	6.2 ± 0.3

[a] Data after 96 h of incubation. Stock solutions in DMSO for all complexes; stock solutions in H_2O for cisplatin. A2780 (cisplatin-sensitive ovarian cancer cells), A2780*cis* (cisplatin-resistant ovarian cancer cells), MDA-MB-231 (triple-negative breast cancer) and U87 (glioblastoma). Data are expressed as mean values ± standard deviation (SD) from measurements performed in triplicate.

Focusing specifically on the series of complexes bearing *N*-acyclic carbene ligands, keeping the substituents R^1 and R^2 on the carbene nitrogen constant, the most active derivatives were those featuring the azulene moiety attached to the carbene nitrogen atom in the 4-position of azulene featuring an *ortho*-fluorophenyl substituent (*e.g.*, **14aa** *vs.* **14ba**, **14ab** *vs.* **14bb**, **14ac** *vs.* **14bc**). When the azulene moiety remains constant, the substituents on the opposite nitrogen that most enhance cytotoxicity include: (i) two ethyl groups (**14aa** and **14ba**), (ii) a pyrrolidine ring (**14ab**), and (iii) a piperidine ring (**14ac**).

Both complexes containing *N*-heterocyclic carbene (NHC) ligands (**16a** and **16b**) also showed high cytotoxicity across the various cancer cell lines tested. Their activity was comparable to that of the most potent *N*-acyclic derivatives (**14aa**, **14ba**, **14ab**, and **14ac**). More specifically, these six lead compounds displayed cytotoxic profiles similar to those of cisplatin in the cisplatin-sensitive ovarian cancer cell line (A2780). Importantly, our compounds demonstrated significantly higher activity than cisplatin against aggressive and treatment-resistant cancer models, including glioblastoma (U87), triple-negative breast cancer (MDA-MB-231), and cisplatin-resistant ovarian cancer (A2780*cis*).

In these models, our six compounds were at least an order of magnitude more active than cisplatin, underscoring their potential to overcome limitations of current chemotherapeutics in hard-to-treat cancers.

Excluding the six previously mentioned compounds that exhibited activity across all tested cancer cell lines, many of the remaining complexes were essentially inactive against tumour cells. Nearly all of these inactive compounds share a common structural feature: the presence of a hydrogen atom bound to both carbene nitrogen atoms (*e.g.*, **14ad**, **14bd**, **14ae**, **14be**, **14af**, **14bf**, **14ag**, and **14bg**).

Interestingly, four other complexes, namely **14ah**, **14bh**, **14ai**, and **14bi**, each containing one *N*-alkyl group such as methyl or *iso*-propyl and one phenyl group attached to the carbene nitrogen, showed selective cytotoxicity in only two or three of the tested cancer cell lines. Notably, their activity was predominantly observed in the more cisplatin-resistant models. This selective behaviour toward hard-to-treat cancers highlights their potential as promising candidates for further development, alongside the six broadly active lead compounds.

Conclusions

Herein, we describe the synthesis of twenty new azulene-tethered gold(I) *N*-acyclic carbene complexes by the template-assisted addition of primary or secondary amines onto gold(I) isonitrile complexes. Alternatively, the synthesis could be performed in a one-pot reaction using commercially available [AuCl(DMS)], an azulene-tethered isonitrile, and an amine. The required isonitriles were prepared from an azulene derivative

obtained by gold-catalyzed dimerization of push–pull bisarylalkynes. The optoelectronic features of these complexes were studied by means of UV-Vis spectroscopy, as well as cyclovoltammetry. The newly synthesized azulene-tethered gold carbene complexes were tested for *in vitro* cytotoxicity against a panel of human cancer cell lines, including both cisplatin-sensitive and -resistant ovarian carcinoma, triple-negative breast cancer, and glioblastoma. A subset of the compounds showed significant anticancer activity, with structure–activity relationship analysis revealing that specific ligand modifications-such as introducing the azulene moiety in its 4-position to the nitrogen atom bound to the carbene unit, the position of the fluorine in the ligand scaffold and ethyl or cyclic groups on the carbene nitrogen-are critical for effectiveness. Six leading compounds, including both *N*-acyclic and *N*-heterocyclic carbene derivatives (**14aa**, **14ba**, **14ab**, **14ac**, **16a** and **16b**) demonstrated cytotoxicity comparable to cisplatin in sensitive models and superior activity-up to an order of magnitude higher-against resistant and aggressive tumours. In contrast, most inactive compounds shared the presence of a hydrogen atom on the carbene nitrogen. Four additional derivatives (**14ah**, **14bh**, **14ai**, and **14bi**) exhibited selective cytotoxicity in only the more treatment-resistant lines, highlighting potential for targeted action. These ten compounds represent the most promising candidates for further investigation in more complex biological systems, such as patient-derived organoids and animal models; alongside the development of gold carbene complexes with similar or enhanced anticancer selectivity.

Author contributions

Martin C. Dietl: conceptualization, investigation, methodology, formal analysis and validation of analytical data, visualisation, writing-original draft; Christopher Hüßler: investigation; Matthias Scherr: investigation; Zoé M. Frederiksen: investigation; Jürgen Graf: data curation, formal analysis; Frank Rominger: data curation, formal analysis, validation and visualisation of X-ray Single Crystal Data; Matthias Rudolph: project administration; Isabella Caligiuri: investigation; Laura Tripodi: investigation; Flavio Rizzolio: investigation, methodology formal analysis and validation of analytical data; Pablo A. Nogara: data curation, formal analysis, validation and visualisation of molecular docking data, writing-review and editing; Laura Orian: data curation, formal analysis, validation and visualisation of DFT data, writing-review and editing; Thomas Scattolin: supervision, writing-original draft, data curation; A. Stephen K. Hashmi: supervision, project administration, resources.

Conflicts of interest

There are no conflicts to declare.

Data availability

CCDC 2449313, 2449314, 2449315, 2449316, 2449317 and 2449318 contain the supplementary crystallographic data for this paper.[64a–f]

The authors declare that all the data used for this manuscript can be found in its supplementary information (SI). Supplementary information is available. See DOI: **https://doi.org/10.1039/d5ra07020a**.

Acknowledgements

M. S. and A. S. K. H. are grateful for the funding by the Hector Fellow Academy.

Notes and references

1 H. Xin, B. Hou and X. Gao, *Acc. Chem. Res.*, 2021, **54**, 1737–1753.
2 J.-X. Dong and H.-L. Zhang, *Chin. Chem. Lett.*, 2016, **27**, 1097–1104.
3 H. Xin, J. Li, X. Yang and X. Gao, *J. Org. Chem.*, 2020, **85**, 70–78.
4 D. Lichosyt, P. Dydio and J. Jurczak, *Chem.–Eur. J.*, 2016, **22**, 17673–17680.
5 G.-O. Buica, I.-G. Lazar, L. Birzan, C. Lete, M. Prodana, M. Enachescu, V. Tecuceanu, A. B. Stoian and E.-M. Ungureanu, *Electrochim. Acta*, 2018, **263**, 382–390.
6 T. Tang, T. Lin, F. Erden, F. Wang and C. He, *J. Mater. Chem. C*, 2018, **6**, 5153–5160.
7 A. G. Lvov and A. Bredihhin, *Org. Biomol. Chem.*, 2021, **19**, 4460–4468.
8 P. Bakun, B. Czarczynska-Goslinska, T. Goslinski and S. Lijewski, *Med. Chem. Res.*, 2021, **30**, 834–846.
9 T. O. Leino, P. Sieger, J. Yli-Kauhaluoma, E. A. Wallén and J. T. Kley, *Eur. J. Med. Chem.*, 2022, **237**, 114374.
10 R. E. Robinson, T. C. Holovics, S. F. Deplazes, G. H. Lushington, D. R. Powell and M. V. Barybin, *J. Am. Chem. Soc.*, 2003, **125**, 4432–4433.
11 J. C. Applegate, M. K. Okeowo, N. R. Erickson, B. M. Neal, C. L. Berrie, N. N. Gerasimchuk and M. V. Barybin, *Chem. Sci.*, 2016, **7**, 1422–1429.
12 P. T. Connelly, J. C. Applegate, D. A. Maldonado, M. K. Okeowo, W. C. Henke, A. G. Oliver, C. L. Berrie and M. V. Barybin, *Dalton Trans.*, 2023, **52**, 11419–11426.
13 R. E. Robinson, T. C. Holovics, S. F. Deplazes, D. R. Powell, G. H. Lushington, W. H. Thompson and M. V. Barybin, *Organometallics*, 2005, **24**, 2386–2397.
14 T. C. Holovics, R. E. Robinson, E. C. Weintrob, M. Toriyama, G. H. Lushington and M. V. Barybin, *J. Am. Chem. Soc.*, 2006, **128**, 2300–2309.
15 M. Fathi-Rasekh, G. T. Rohde, M. D. Hart, T. Nakakita, Y. V. Zatsikha, R. R. Valiev, M. V. Barybin and V. N. Nemykin, *Inorg. Chem.*, 2019, **58**, 9316–9325.
16 S. Sun, X. Zhuang, L. Wang, B. Zhang, J. Ding, F. Zhang and Y. Chen, *J. Mater. Chem. C*, 2017, **5**, 2223–2229.

17 E. de Domingo, M. Barcenilla, J. M. Martín-Alvarez, J. A. Miguel and S. Coco, *Dyes Pigm.*, 2020, **176**, 108195.
18 D. L. DuBose, R. E. Robinson, T. C. Holovics, D. R. Moody, E. C. Weintrob, C. L. Berrie and M. V. Barybin, *Langmuir*, 2006, **22**, 4599–4606.
19 C. Yang, K. S. Schellhammer, F. Ortmann, S. Sun, R. Dong, M. Karakus, Z. Mics, M. Löffler, F. Zhang, X. Zhuang, E. Cánovas, G. Cuniberti, M. Bonn and X. Feng, *Angew. Chem., Int. Ed.*, 2017, **56**, 3920–3924.
20 T. R. Maher, A. D. Spaeth, B. M. Neal, C. L. Berrie, W. H. Thompson, V. W. Day and M. V. Barybin, *J. Am. Chem. Soc.*, 2010, **132**, 15924–15926.
21 E. de Domingo, M. Bardají, G. García and S. Coco, *Dyes Pigm.*, 2024, **226**, 112149.
22 G. Rouschias and B. Shaw, *J. Chem. Soc. D*, 1970, 183.
23 G. Rouschias and B. Shaw, *J. Chem. Soc.*, 1971, 2097–2104.
24 L. Tschugajeff, M. Skanawy-Grigorjewa, A. Posnjak and M. Skanawy-Grigorjewa, *Z. Anorg. Allg. Chem.*, 1925, **148**, 37–42.
25 F. Bonati and G. Minghetti, *Synth. React. Inorg. Met. Org. Chem.*, 1971, **1**, 299–302.
26 F. Bonati and G. Minghetti, *J. Organomet. Chem.*, 1973, **59**, 403–410.
27 G. Minghetti and F. Bonati, *J. Organomet. Chem.*, 1973, **54**, C62–C63; F. Bonati and G. Minghetti, *Inorg. Chim. Acta*, 1974, **9**, 95–112.
28 E. Ansari, R. Kumar and A. Ratnam, *Dalton Trans.*, 2025, **54**, 7553–7601.
29 B. Bertrand, A. Citta, I. L. Franken, M. Picquet, A. Folda, V. Scalcon, M. P. Rigobello, P. Le Gendre, A. Casini, E. Bodio and J. Biol, *Inorg. Chem.*, 2015, **20**, 1005–1020.
30 E. Bortolamiol, F. Visentin and T. Scattolin, *Appl. Sci.*, 2023, **13**, 5561.
31 M. Safir Filho, T. Scattolin, P. Dao, N. V. Tzouras, R. Benhida, M. Saab, K. Van Hecke, P. Lippmann, A. R. Martin, I. Ott and S. P. Nolan, *New J. Chem.*, 2021, **45**, 9995–10001.
32 N. V. Tzouras, T. Scattolin, A. Gobbo, S. Bhandary, F. Rizzolio, E. Cavarzerani, V. Canzonieri, K. Van Hecke, G. C. Vougioukalakis, C. S. J. Cazin and S. P. Nolan, *ChemMedChem*, 2022, **17**, e202200135.
33 T. Scattolin, P. Lippmann, M. Beliš, K. van Hecke, I. Ott and S. P. Nolan, *Appl. Organomet. Chem.*, 2024, **38**, e6624.
34 T. Scattolin, G. Tonon, E. Botter, S. G. Guillet, N. V. Tzouras and S. P. Nolan, *Chem.–Eur. J.*, 2023, **29**, e202301961.
35 J. Saez, J. Quero, M. J. Rodriguez-Yoldi, M. C. Gimeno and E. Cerrada, *Inorg. Chem.*, 2024, **63**, 19769–19782.
36 M. Gil-Moles, M. E. Olmos, J. M. López-de-Luzuriaga, I. Ott and M. Concepción Gimeno, *Inorg. Chem. Front.*, 2024, **11**, 4802–4814.
37 M. Gil-Moles and M. Concepción Gimeno, *ChemMedChem*, 2024, **19**, e202300645.
38 J. Quero, J. C. Royo, B. Fodor, M. C. Gimeno, J. Osada, M. J. Rodríguez-Yoldi and E. Cerrada, *Biomedicines*, 2022, **10**, 1437.
39 R. Rubbiani, I. Kitanovic, H. Alborzinia, S. Can, A. Kitanovic, L. A. Onambele, M. Stefanopoulou, Y. Geldmacher, W. S. Sheldrick, G. Wolber, A. Prokop, S. Wölfl and I. Ott, *J. Med. Chem.*, 2010, **53**, 8608–8618.
40 M. Mora, M. C. Gimeno and R. Visbal, *Chem. Soc. Rev.*, 2019, **48**, 447–462.
41 V. Vethacke, V. Claus, M. C. Dietl, D. Ehjeij, A. Meister, J. F. Huber, L. K. Paschai Darian, M. Rudolph, F. Rominger and A. S. K. Hashmi, *Adv. Synth. Catal.*, 2022, **364**, 536–554.
42 M. C. Dietl, V. Vethacke, A. Keshavarzi, F. F. Mulks, F. Rominger, M. Rudolph, I. A. I. Mkhalid and A. S. K. Hashmi, *Organometallics*, 2022, **41**, 802–810.
43 M. C. Dietl, M. Maag, S. Ber, F. Rominger, M. Rudolph, I. Caligiuri, P. K. Andele, I. A. I. Mkhalid, F. Rizzolio, P. A. Nogara, L. Orian, T. Scattolin and A. S. K. Hashmi, *Chem. Sci.*, 2024, **15**, 15291–15298.
44 A. S. K. Hashmi, T. Hengst, C. Lothschütz and F. Rominger, *Adv. Synth. Catal.*, 2010, **352**, 1315–1337.
45 A. S. K. Hashmi, C. Lothschütz, C. Böhling, T. Hengst, C. Hubbert and F. Rominger, *Adv. Synth. Catal.*, 2010, **352**, 3001–3012.
46 A. S. K. Hashmi, C. Lothschütz, K. Graf, T. Häffner, A. Schuster and F. Rominger, *Adv. Synth. Catal.*, 2011, **353**, 1407–1412.
47 A. S. K. Hashmi, C. Lothschütz, C. Böhling and F. Rominger, *Organometallics*, 2011, **30**, 2411–2417.
48 D. Riedel, T. Wurm, K. Graf, M. Rudolph, F. Rominger and A. S. K. Hashmi, *Adv. Synth. Catal.*, 2015, **357**, 1515–1523.
49 T. Wurm, F. Mulks, C. R. N. Böhling, D. Riedel, P. Zargaran, M. Rudolph, F. Rominger and A. S. K. Hashmi, *Organometallics*, 2016, **35**, 1070–1078.
50 C. Lothschütz, T. Wurm, A. Zeiler, A. F. v. Falkenhausen, M. Rudolph, F. Rominger and A. S. K. Hashmi, *Chem.–Asian J.*, 2016, **11**, 342–346.
51 P. Zargaran, T. Wurm, D. Zahner, J. Schießl, M. Rudolph, F. Rominger and A. S. K. Hashmi, *Adv. Synth. Catal.*, 2018, **360**, 106–111.
52 A. Cervantes-Reyes, F. Rominger, M. Rudolph and A. S. K. Hashmi, *Adv. Synth. Catal.*, 2020, **362**, 2523–2533.
53 R. Manzano, F. Rominger and A. S. K. Hashmi, *Organometallics*, 2013, **32**, 2199–2203.
54 A. Cervantes-Reyes, F. Rominger, M. Rudolph and A. S. K. Hashmi, *Chem.–Eur. J.*, 2019, **25**, 11745–11757.
55 H. Seo, B. P. Roberts, K. A. Abboud, K. M. Merz and S. Hong, *Org. Lett.*, 2010, **12**, 4860–4863.
56 V. Claus, M. Schukin, S. Harrer, M. Rudolph, F. Rominger, A. M. Asiri, J. Xie and A. S. K. Hashmi, *Angew. Chem., Int. Ed.*, 2018, **57**, 12966–12970.
57 S. M. Creedon, H. Kevin Crowley and D. G. McCarthy, *J. Chem. Soc., Perkin Trans. 1*, 1998, 1015–1018.
58 A. Porcheddu, G. Giacomelli and M. Salaris, *J. Org. Chem.*, 2005, **70**, 2361–2363.
59 J. Zhu, X. Wu and S. J. Danishefsky, *Tetrahedron Lett.*, 2009, **50**, 577–579.
60 X. Wang, Q.-G. Wang and Q.-L. Luo, *Synth.*, 2015, **47**, 49–54.
61 H. Schmidbaur, *Gold Bull*, 2000, **33**, 3–10.
62 H. Schmidbaur, *Chem. Soc. Rev.*, 1995, **24**, 391–400.
63 H. Schmidbaur and A. Schier, *Chem. Soc. Rev.*, 2012, **41**, 370–412.

64 (*a*) CCDC 2449313: Experimental Crystal Structure Determination, 2025, DOI: 10.5517/ccdc.csd.cc2n6q3q; (*b*) CCDC 2449314: Experimental Crystal Structure Determination, 2025, DOI: 10.5517/ccdc.csd.cc2n6q4r; (*c*) CCDC 2449315: Experimental Crystal Structure Determination, 2025, DOI: 10.5517/ccdc.csd.cc2n6q5s; (*d*) CCDC 2449316: Experimental Crystal Structure Determination, 2025, DOI: 10.5517/ccdc.csd.cc2n6q6t; (*e*) CCDC 2449317: Experimental Crystal Structure Determination, 2025, DOI: 10.5517/ccdc.csd.cc2n6q7v; (*f*) CCDC 2449318: Experimental Crystal Structure Determination, 2025, DOI: 10.5517/ccdc.csd.cc2n6q8w.